Science Advances
AAAS

Supplementary Materials for

Much more to explore with an oxidation state of nearly four: Pr valence instability in intermetallic *m*-$Pr_2Co_3Ge_5$

Trent M. Kyrk *et al.*

Corresponding author: Julia Y. Chan, julia_chan@baylor.edu

Sci. Adv. **10**, eadl2818 (2024)
DOI: 10.1126/sciadv.adl2818

This PDF file includes:

The $Lu_2Co_3Si_5$ and $U_2Co_3Si_5$ Structure Types

The $Lu_2Co_3Si_5$ (*I*2/*c*) and $U_2Co_3Si_5$ (*Ibam*) (*24*) structure types are distorted coloring variants of the $BaAl_4$ structure type (*59*), representing the compositional and structural intermediate to the $BaNiSn_3$ (*I*4*mm*) and $CaBe_2Ge_2$ (*P*4/*nmm*) structure types (*60*). The slabs are linked via a five-coordinate square pyramidal main-group or transition metal that creates a three-dimensional framework surrounding planar square layers of A atoms. The $[Co_3Ge_5]$ tetrahedral slab is distorted from the alternating assignment of M and X such that they are not perfectly aligned and are corrugated (Fig. 1e – 1h). The consequence of the tetrahedral corrugation is that the A layers are not planar or square, and instead form "wavy planes" (*61*).

The $Lu_2Co_3Si_5$ (*I*2/*c*) structure type is related to the $U_2Co_3Si_5$ (*Ibam*) structure type by a monoclinic deformation (*25*). The $Lu_2Co_3Si_5$ structure type is referenced in the pseudo-orthorhombic setting (*I*2/*c*) related to the standard setting (*C*2/*c*) by the transformation matrix $(101/0\bar{1}0/00\bar{1})$ for this discussion to facilitate comparison with the $U_2Co_3Si_5$ type structure. The second coordination sphere of the tetrahedral transition metal environment can be used to understand how the monoclinic deformation takes place. In $U_2Co_3Si_5$ type structures, the tetrahedral transition metal site exists in a "4 + 2" coordination, where the first coordination sphere is a tetrahedral environment of equidistant main group metals, and the second coordination sphere forms a distorted octahedral environment with two additional main group metals spaced further away. When the monoclinic distortion is present (*25*), the transition metal coordination environment approaches a "5 + 1" geometry through a "push-pull" type distortion dependent upon the degree of distortion, where β has been observed as large as 92.6°. Here, one axial main group metal becomes equidistant to the tetrahedral environment and the other becomes increasingly distant (*23*). The distortion also corresponds to the dimerization of the five-coordinate transition metal site along the crystallographic *c*-direction. Together, these changes in the 3-dimensional framework result in the reduction in point symmetry of the lanthanide site from C_s to C_1, potentially impactful to the crystal field splitting of 4*f* orbitals. The non-linear behavior coincides with the deformation in the second coordination sphere of the Co1 local environment.

Upon completion of the second order structural phase transformation at $T = 343$ K in *m*-$Pr_2Co_3Ge_5$, the tetrahedral Ge2 and Ge4 atomic sites that were unique at room temperature become symmetrically equivalent. In the $[Co_3Ge_5]$ slab, the intermediate "5 + 1" geometry of the Co1

second coordination sphere increases symmetry to a "4 + 2" geometry with $d_{Co1\text{-}Ge3}$ = 2.4395(14) Å x2, $d_{Co1\text{-}Ge3}$ = 2.4493(12) Å x2, $d_{Co1\text{-}Ge4}$ = 2.655(2) Å, and $d_{Co1\text{-}Ge2}$ = 2.764(2) Å in room temperature *m*-$Pr_2Co_3Ge_5$ converging to $d_{Co1\text{-}Ge3}$ = 2.4419(6) Å x4 and $d_{Co1\text{-}Ge2}$ = 2.7166(9) Å x2 in the high temperature transformed structure. Notably, the five coordinate Co2 atoms that were dimerized along the *c*-direction at room temperature undergo the largest change in bond distance within the framework, expanding from $d_{Co2\text{-}Co2}$ = 3.464(2) Å to $d_{Co2\text{-}Co2}$ = 3.5838(7) Å at 343 K. While the loss of dimerization of the Co2 sites and convergence of the Co1-Ge distances may seem isolated, they are explicitly linked through a scissor gate folding mechanism: as the Ge atoms converge, the Co2 sites are separated. Such behavior has been seen in other lanthanide intermetallic compounds containing Group 9 transition metals like in the structural phase transformation of CeRhGe (*46*) and the charge density wave transformation in $A_2Ir_3Si_5$ (A = Ho, Er, Lu) (*33-35*).

At room temperature, the shortest Pr-Ge interatomic distance in *m*-$Pr_2Co_3Ge_5$, $d_{Pr\text{-}Ge3}$ = 2.9489(11) Å, is far shorter than distances observed in similar compounds $PrCoGe_3$ ($d_{Pr\text{-}Ge1}$ = 3.120(1) Å) (*62*) and $PrCo_2Ge_2$ ($d_{Pr\text{-}Ge}$ = 3.153(14) Å) (*63*) and shorter than the sum of the single bond covalent radii of Pr and Ge $d^{calc}_{Pr\text{-}Ge}$=2.97 Å (*64*). The only other reported Pr-Co-Ge ternary with Pr-Ge bonds shorter than the sum of their covalent radii is $Pr_{117}Co_{56.7}Ge_{112}$ and no Pr-Ge binaries exhibit such distances, including those synthesized at high-pressure (*65-67*). Interestingly, the short A-X distance seems to be a feature of the early lanthanide compounds across multiple $A_2M_3X_5$ structure types (*64*). The next eight Pr-Ge bond distances are longer, $d_{Pr\text{-}Ge}$ = 3.1275(17) – 3.2004(8) Å, and correspond more closely with what is observed in $PrCoGe_3$ (*62*) and $PrCo_2Ge_2$ (*63*), with the remaining Pr-Ge contact having a distance of $d_{Pr\text{-}Ge3}$ = 3.2816(11) Å. At 343 K, the Pr-Ge3 distances are relatively invariant, with the shortest, $d_{Pr\text{-}Ge3}$ = 2.9443(10) Å, and longest, $d_{Pr\text{-}Ge3}$ = 3.2839(10) Å, distances showing little change from the room temperature structure.

While few structures within the $A_2M_3X_5$ family have been investigated as a function of temperature, structural phase transformation are not common. Neutron diffraction data from compounds isotypic to $Lu_2Co_3Si_5$ (*I*2/*c*) either report no temperature dependent anomalies in structure, such as in $A_2Co_3Si_5$ (A = Tb, Dy), or report minimal changes in the angle β, such as in $U_2Rh_3Si_5$. Examples of compounds in the space group *Ibam* obtained from powder neutron diffraction, namely $A_2Ni_3Si_5$ (A = Ce, Pr, Nd, Tb, Dy) (*68*), $Tb_2Ir_3Si_5$ (*69*), $Ce_2Ni_3Ge_5$ (*70*), and $Pr_2Pd_3Ge_5$ (*71*), indicate that not all compounds of the $U_2Co_3Si_5$ structure type undergo a low

temperature monoclinic deformation. Additionally, the structural phase transformation of *m*-$Pr_2Co_3Ge_5$ is reversible (Fig. S2).

Powder X-ray Diffraction

Table S1. Atomic Positions of Room Temperature *m*-$Pr_2Co_3Ge_5$ and *o*-$Pr_2Co_3Ge_5$ obtained from Rietveld Refinement. *Atomic displacement parameters were obtained from single crystal X-ray diffraction and were not refined.

Atom	Wyckoff site	*x*	*y*	*z*	$B_{iso}(Å^2)^*$
RT *m*-$Pr_2Co_3Ge_5$ (Space group: *I*2/*c*)					
Pr	8*f*	0.26477 (5)	0.13473 (5)	0.26496 (14)	0.536117
Co1	4*e*	0	0.00212 (17)	¼	0.634023
Co2	8*f*	0.10313 (11)	0.36109 (10)	0.1113 (3)	0.802201
Ge1	4*e*	0	0.50300 (14)	¼	0.626917
Ge2	4*e*	0	0.77049 (13)	¼	0.660869
Ge3	8*f*	0.33909 (10)	0.40284 (8)	0.3374 (2)	0.602441
Ge4	4*e*	0	0.22454 (13)	¼	0.650604
343 K *m*-$Pr_2Co_3Ge_5$ (Space group: *Ibam*)					
Pr	8*j*	0.26489 (4)	0.13432 (4)	0	0.533748
Co1	4*a*	0	0	¼	0.632444
Co2	8*j*	0.10475 (10)	0.36120 (9)	0	0.821151
Ge1	4*b*	½	0	¼	0.622180
Ge2	8*g*	0	0.22795 (7)	¼	0.673502
Ge3	8*j*	0.33878 (9)	0.40271 (6)	0	0.600072
As-grown *o*-$Pr_2Co_3Ge_5$ (Space group: *Ibam*)					
Pr	8*j*	0.26453 (4)	0.13419 (4)	0	0.533748
Co1	4*a*	0	0	¼	0.632444
Co2	8*j*	0.10515 (9)	0.36144 (9)	0	0.821151
Ge1	4*b*	½	0	¼	0.622180
Ge2	8*g*	0	0.22795 (7)	¼	0.673502
Ge3	8*j*	0.33961 (8)	0.40295 (6)	0	0.600072

Table S2. Bond Distances of the Pr Local Environment (Å) in Room Temperature *m*-$Pr_2Co_3Ge_5$, 343 K *m*-$Pr_2Co_3Ge_5$, and, for Comparison, As-grown *o*-$Pr_2Co_3Ge_5$.

		RT *m*-$Pr_2Co_3Ge_5$ (*I*2/*c*)	343 K *m*-$Pr_2Co_3Ge_5$ (*Ibam*)	As-grown *o*-$Pr_2Co_3Ge_5$ (*Ibam*)
Pr:	Pr	4.0216 (11)	4.0346 (6)	4.0349 (5)
	Pr	4.0290 (11)	-	-
	Pr	4.3464 (11)	4.3414 (6)	4.3370 (5)
	Ge1	3.1417 (11)	3.1684 (5)	3.1699 (4)
	Ge1	3.1981 (10)	-	-
	Ge2	3.1661 (11)	3.1907 (7)	3.1922 (6)
	Ge2/4	3.2167 (10)	-	-
	Ge2	3.2004 (8)	3.1853 (6)	3.1843 (5)
	Ge2/4	3.1551 (9)	-	-
	Ge3	2.9489 (11)	2.9443 (10)	2.9394 (9)
	Ge3	3.1275 (17)	3.1305 (4)	3.1338 (3)
	Ge3	3.1300 (14)	-	-
	Ge3	3.2816 (11)	3.2851 (10)	3.2867 (9)
	Co2	3.1330 (13)	3.1301 (13)	3.1279 (11)
	Co2	3.1657 (18)	3.1952 (4)	3.1969 (4)
	Co2	3.2326 (21)	-	-
Co1:	Ge2	2.764 (3)	2.7174 (10)	2.7166 (8)
	Ge3	2.4411 (16)	2.4483 (8)	2.4419 (6)
	Ge3	2.4476 (13)	-	-
	Ge4	2.654 (3)	-	-
	Co1	2.92449 (5)	2.92731 (1)	2.92904 (1)
Co2:	Ge1	2.4207 (19)	2.4386 (9)	2.4367 (8)
	Ge1	2.4421 (18)	-	-
	Ge2	2.4081 (17)	2.3949 (11)	2.3962 (10)
	Ge2/4	2.3764 (19)	-	-
	Ge3	2.3690 (15)	2.3500 (14)	2.3547 (12)

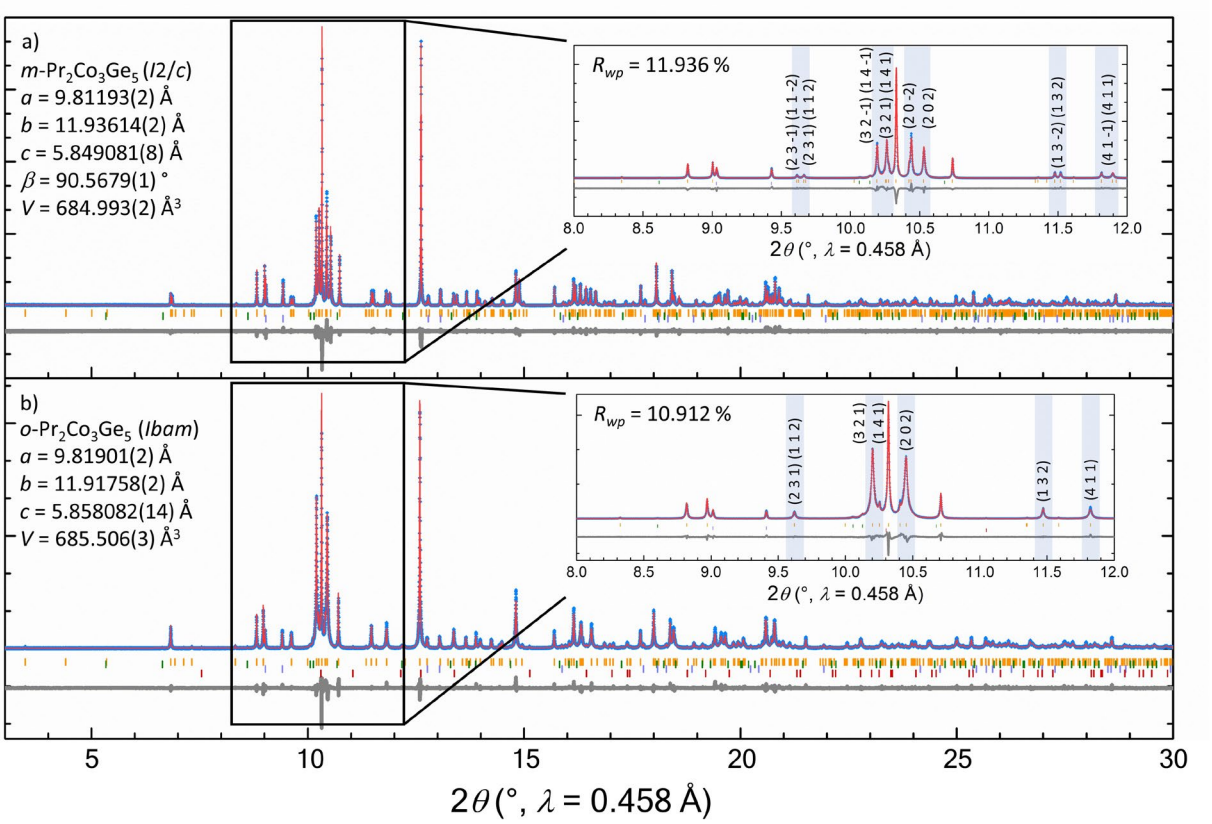

Figure S1. High resolution powder X-ray diffraction of (a) *m*-$Pr_2Co_3Ge_5$ and (b) *o*-$Pr_2Co_3Ge_5$. Observed data, Rietveld refinement, and difference curves are shown in blue, red, and grey, respectively. Tick marks of $Pr_2Co_3Ge_5$, $PrCoGe_3$, Sn, and Al_2O_3 are shown in orange, green, purple, and red, respectively. The insets highlight splitting of select reflections corresponding to a loss in symmetry with *m*-$Pr_2Co_3Ge_5$ indexed in the unconventional space group setting *I*2/*c*. The lattice parameters of *m*-$Pr_2Co_3Ge_5$ in the standard setting *C*2/*c* are a = 11.37315(2) Å, b = 11.93614(2) Å, c = 5.849081(8) Å, β = 120.3803(1) °, V = 684.993(2) Å^3.

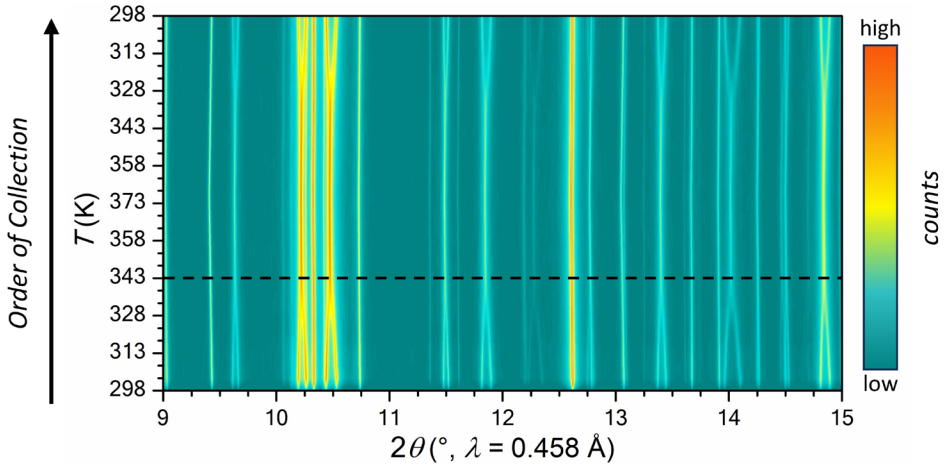

Figure S2. Contour plot of temperature dependent X-ray diffraction data of *m*-$Pr_2Co_3Ge_5$ as obtained from high resolution powder X-ray diffraction. The temperature of phase transformation is given with the dashed black line.

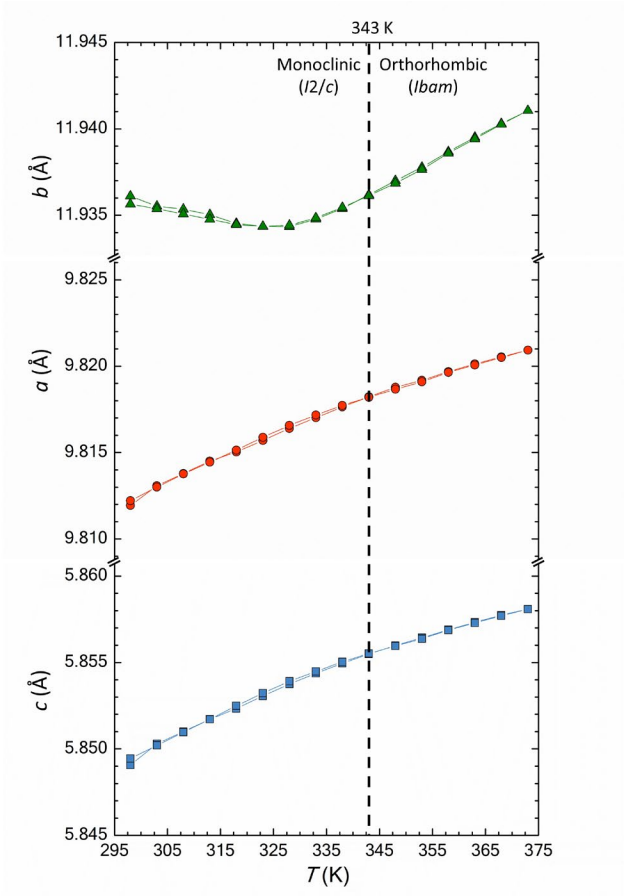

Figure S3. The temperature dependent lattice parameters of *m*-$Pr_2Co_3Ge_5$ as obtained from high resolution powder X-ray diffraction. Lattice parameters *a*, *b*, and *c* are given as red, green, and blue, respectively.

Room Temperature Electron-Energy Loss Spectroscopy

Monochromated EEL spectra were collected for both polymorphs from the Pr $M_{4,5}$ and the Co $L_{2,3}$ energy ranges (Figs. 2a and 2b, respectively). For Pr, there are two dominant edges with peaks at 928.1 and 947.9 eV, corresponding to the dipole-allowed transitions from $3d^{5/2}$ to $4f^{7/2}$ and $3d^{3/2}$ to $4f^{5/2}$, respectively. The M_5:M_4 edge height ratio increases from 1.6:1 to 1.72:1 and the total integrated area, which serves as a measure of unoccupied density of states (shaded area in Fig. 2c), decreases from 8.24 to 6.81 eV*counts when comparing the room temperature and high temperature structures. A chemical shift is not observed in Pr as the edge onset is similar between the monoclinic and orthorhombic polymorphs; however, there is a dramatic difference in valency, with *m*-$Pr_2Co_3Ge_5$ predominantly Pr^{4+} (Pr^{n+}, n = 3.80(5)) and *o*-$Pr_2Co_3Ge_5$ predominantly Pr^{3+} (Pr^{n+}, n = 3.00(5)) based on MLLS fits and reference spectra (see Methods). Since only one crystallographically unique Pr atomic site exists in both polymorphs of $Pr_2Co_3Ge_5$, the oxidation state of Pr must be in an intermediate valence state in *m*-$Pr_2Co_3Ge_5$. Pr was observed to be weakly tetravalent in $PrFe_{10}Mo_2$ and $PrNi_5$ based on X-ray absorption spectroscopy, with valences of 3.08(3) and 3.10(3) respectively (*72*), but this is far less than what is observed in *m*-$Pr_2Co_3Ge_5$.

Like Pr, the Co $L_{2,3}$ edges result from dipole allowed electron transitions; however, for cobalt, these transitions are from the $2p^{3/2}$ to $3d^{5/2}$ states and the $2p^{1/2}$ to $3d^{3/2}$ states. The edge onset for both polymorphs is similar with the onset slightly lower in *m*-$Pr_2Co_3Ge_5$ (775.06 eV) compared to *o*-$Pr_2Co_3Ge_5$ (775.10 eV). The Co $L_{2,3}$ edge onset is lower for the orthorhombic structure when compared to the monoclinic structure, implying that the orthorhombic 3*d* Co electrons possess a lower ionization energy threshold compared to their monoclinic counterparts. In other words, the orthorhombic crystal structure facilitates removal of electrons from the 3*d* orbitals of Co atoms, resulting in a lower energy requirement for ionization compared to the monoclinic crystal structure. Additionally, the small high energy shift of the Co $L_{2,3}$ edge onsets in *m*-$Pr_2Co_3Ge_5$ compared to *o*-$Pr_2Co_3Ge_5$ suggest a slightly higher oxidation state of the monoclinic Co. However, the Co $L_{2,3}$ edge maxima in *o*-$Pr_2Co_3Ge_5$ are at higher energies compared to the monoclinic structure. The intensity of the peaks reflects the occupancy of the relevant orbitals, while the shape informs on hybridization and interactions between the electronic orbitals involved in the orbital transitions. Broader edges are indicative of more rapid decay processes, suggesting that *m*-$Pr_2Co_3Ge_5$ contains more unoccupied 3*d* states compared to *o*-$Pr_2Co_3Ge_5$.

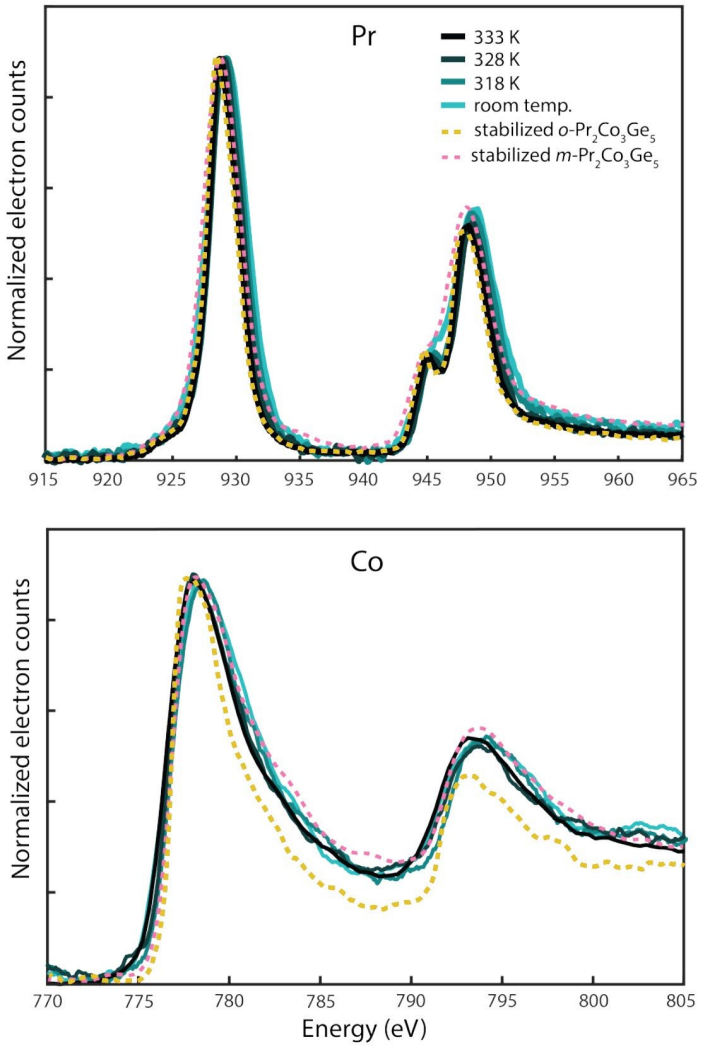

Figure S4. Temperature dependent EEL spectra across the structural phase transformation of *m*-$Pr_2Co_3Ge_5$ overlayed for feature comparison. Data were normalized based on the M_5 or L_3 edge maxima.

Field Dependent and Temperature Dependent Magnetic Measurements

For the orthorhombic polymorph, temperature dependent magnetic susceptibility measurements along the *a-, b-,* and *c*-crystallographic directions result in one magnetic transition above $H = 0.2$ T. With an applied field of $H \geq 0.2$ T parallel to the *a*-direction, a single broad magnetic transition is visible at $T_{sp} = 32.5$ K (Fig. S5a); however, at reduced fields of $H = 0.05$ T, this magnetic transition shifts to $T_{sp} = 30.8$ K and a second feature emerges at $T_M = 3.4$ K (Fig. S5). With field applied parallel to either the *b*- or *c*-directions, two magnetic transitions are present for all fields at $T_{sp} \sim 32$ K and $T_M = 3.2$ K or $T_M = 10$ K, respectively. Unlike the transitions observed along the *a*-direction, the magnitude of magnetic ordering along the *b*- and *c*-directions are strongest at T_M, with ordering along the *c*-direction being significantly more pronounced than the other directions. Additionally, with magnetic fields applied parallel to the *a*-direction, there is a slight bifurcation of the zero field-cooled and field-cooled magnetization below $T = 4$ K for $H = 0.05$ and 0.5, but no difference is observed for fields applied along the *b*- and *c*-directions. Compared to the magnetic susceptibility of *o*-$Pr_2Co_3Ge_5$ with a magnetic field of $H = 0.2$ T applied along the *a*-direction, the first transition in *m*-$Pr_2Co_3Ge_5$ occurs at a higher temperature of $T_{sp} = 35.3$ K and an additional magnetic transition is observed at $T_M = 10$ K. The magnetic ordering event with field applied along the *c*-direction also shows a shift towards higher temperature ($T_{sp} = 34.8$ K).

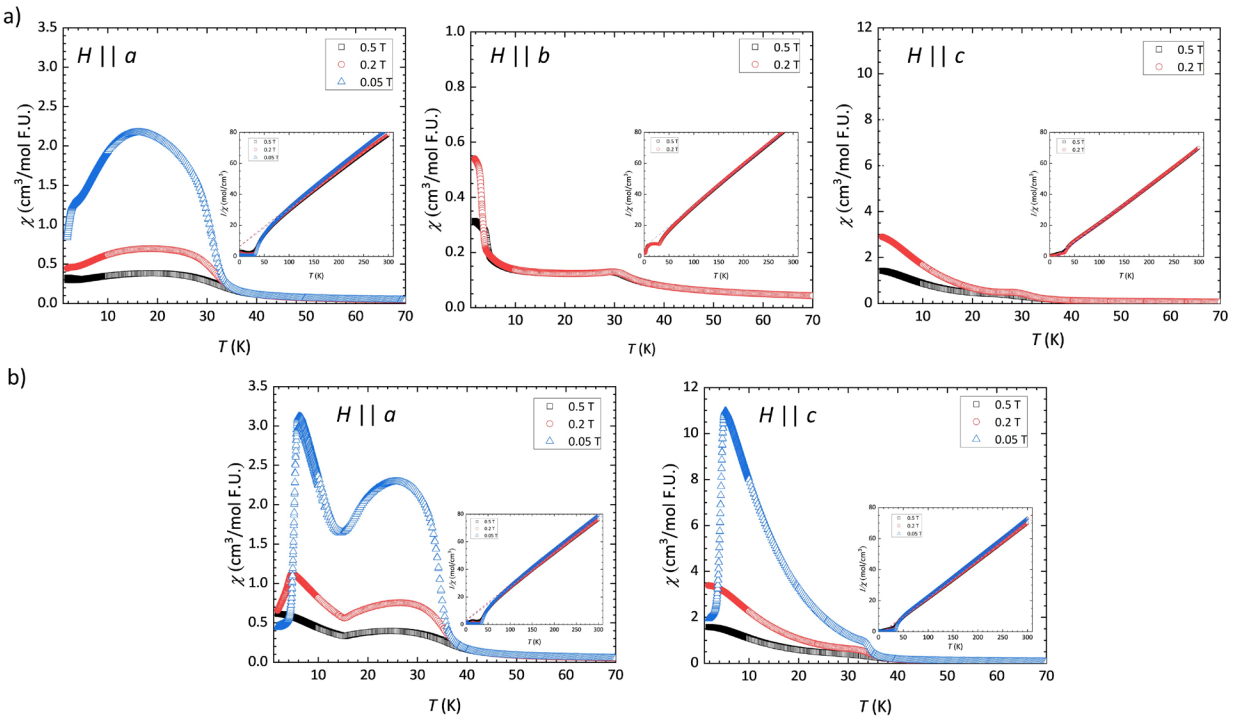

Figure S5. Temperature dependent magnetization of (a) *o*-$Pr_2Co_3Ge_5$ and (b) *m*-$Pr_2Co_3Ge_5$ at applied fields of 0.05 T (blue), 0.2 T (red), and 0.5 T (black).

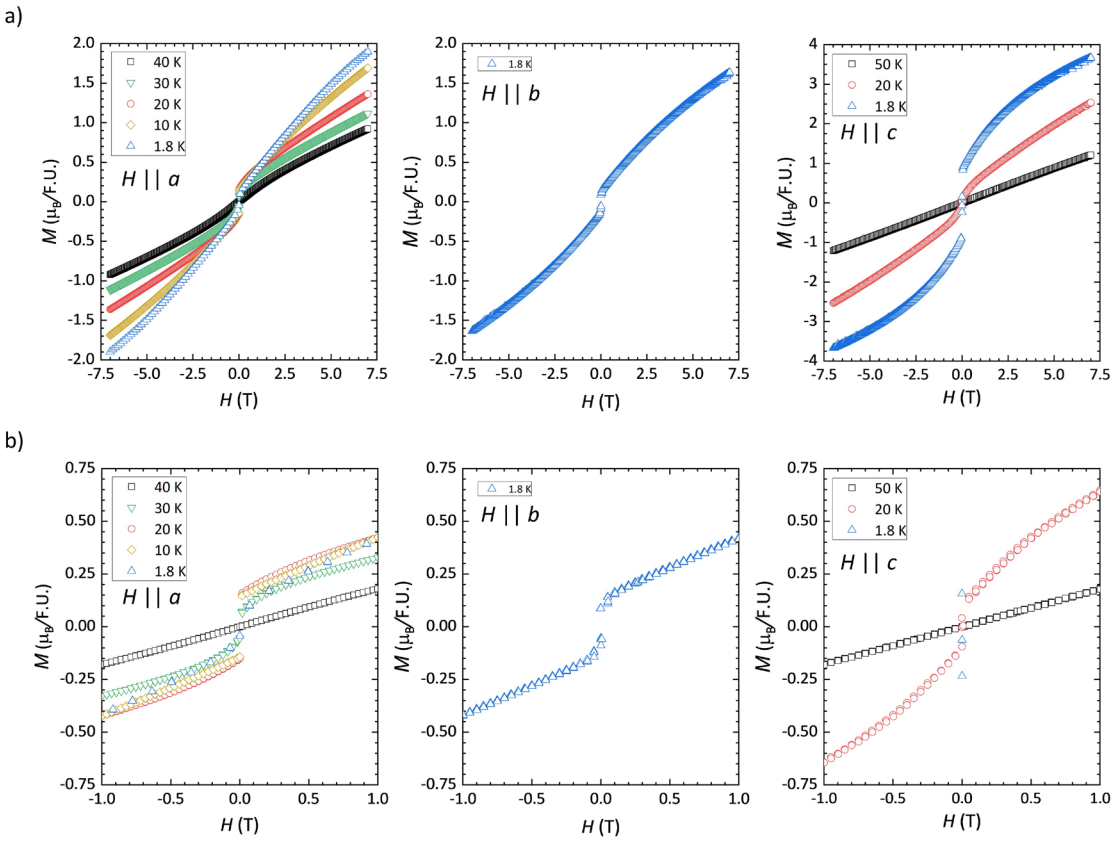

Figure S6. Field dependent magnetization of *o*-$Pr_2Co_3Ge_5$ with (a) the applied fields from -7.5 to 7.5 T and (b) -1 T to 1 T.

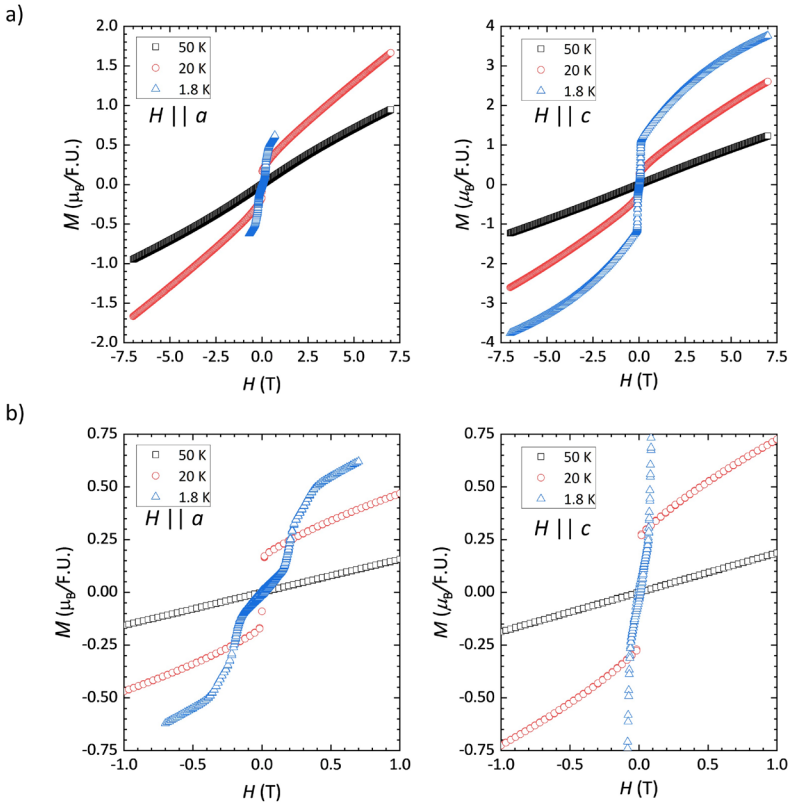

Figure S7. Field dependent magnetization of *m*-$Pr_2Co_3Ge_5$ with (a) the applied fields from -7.5 to 7.5 T and (b) - 1 T to 1 T.

Table S3. Summarized Magnetic Susceptibility for *o*-$Pr_2Co_3Ge_5$ and *m*-$Pr_2Co_3Ge_5$

	Applied Field (T)	μ_{eff} (μ_B Pr^{-1})	μ_{eff} (μ_B F.U.$^{-1}$)	θ_{CW} (K)	T_{sp} (K)	T_M (K)
o-$Pr_2Co_3Ge_5$	*H* // *a*; 0.5	4.05 (1)	5.72 (2)	-25.5 (2)	32.5	-
	0.2	4.03 (1)	5.70 (2)	-25.7 (1)	31.9	-
	0.05	3.95 (1)	5.58 (1)	-25.4 (1)	30.8	3.4
	H // *b*; 0.5	3.87 (1)	5.47 (1)	-22.6 (1)	31.9	4.3
	0.2	3.86 (1)	5.46 (1)	-22.6 (1)	32.3	3.2
	H // *c*; 0.5	4.04 (1)	5.72 (1)	13.4 (1)	31.9	10
	0.2	4.04 (1)	5.71 (1)	13.5 (1)	31.3	10
m-$Pr_2Co_3Ge_5$	*H* // *a*; 0.5	4.02 (1)	5.68 (1)	-10.4 (1)	36.4	10
	0.2	4.02 (1)	5.68 (1)	-11.0 (1)	35.3	10
	0.05	3.95 (1)	5.58 (1)	-12.3 (1)	34.5	10
	H // *c*; 0.5	4.05 (1)	5.72 (1)	12.2 (1)	35.7	10
	0.2	4.05 (1)	5.73 (1)	11.3 (1)	34.8	10
	0.05	3.97 (1)	5.62 (1)	10.2 (1)	34.4	10

REFERENCES AND NOTES

1. Y.-F. Yang, An emerging global picture of heavy fermion physics. *J. Phys. Condens. Matter* **35**, 103002 (2022).

2. S. E. Grefe, H.-H. Lai, S. Paschen, Q. Si, Weyl-Kondo semimetals in nonsymmorphic systems. *Phys. Rev. B* **101**, 075138 (2020).

3. L. Chen, C. Setty, H. Hu, M. G. Vergniory, S. E. Grefe, L. Fischer, X. Yan, G. Eguchi, A. Prokofiev, S. Paschen, J. Cano, Q. Si, Topological semimetal driven by strong correlations and crystalline symmetry. *Nat. Phys.* **18**, 1341–1346 (2022).

4. W. Witczak-Krempa, G. Chen, Y. B. Kim, L. Balents, Correlated quantum phenomena in the strong spin-orbit regime. *Annu. Rev. Condens. Matter Phys.* **5**, 57–82 (2014).

5. H. Zhao, J. Zhang, M. Lyu, S. Bachus, Y. Tokiwa, P. Gegenwart, S. Zhang, J. Cheng, Y.-F. Yang, G. Chen, Y. Isikawa, Q. Si, F. Steglich, P. Sun, Quantum-critical phase from frustrated magnetism in a strongly correlated metal. *Nat. Phys.* **15**, 1261–1266 (2019).

6. M. Kavai, J. Friedman, K. Sherman, M. Gong, I. Giannakis, S. Hajinazar, H. Hu, S. E. Grefe, J. Leshen, Q. Yang, S. Nakatsuji, A. N. Kolmogorov, Q. Si, M. Lawler, P. Aynajian, Inhomogeneous Kondo-Lattice in geometrically frustrated Pr2Ir2O7. *Nat. Commun.* **12**, 1377 (2021).

7. F. Giustino, J. H. Lee, F. Trier, M. Bibes, S. M. Winter, R. Valentí, Y.-W. Son, L. Taillefer, C. Heil, A. I. Figueroa, B. Plaçais, Q. Wu, O. V. Yazyev, E. P. A. M. Bakkers, J. Nygård, P. Forn-Díaz, S. De Franceschi, J. W. McIver, L. E. F. F. Torres, T. Low, A. Kumar, R. Galceran, S. O. Valenzuela, M. V. Costache, A. Manchon, E.-A. Kim, G. R. Schleder, A. Fazzio, S. Roche, The 2021 quantum materials roadmap. *J. Phys. Mater.* **3**, 042006 (2020).

8. H. Q. Yuan, F. M. Grosche, M. Deppe, C. Geibel, G. Sparn, F. Steglich, Observation of two distinct superconducting phases in CeCu2Si2. *Science* **302**, 2104–2107 (2003).

9. R. T. Macaluso, S. Nakatsuji, K. Kuga, E. L. Thomas, Y. Machida, Y. Maeno, Z. Fisk, J. Y. Chan, Crystal structure and physical properties of polymorphs of LnAlB4 (Ln = Yb, Lu). *Chem. Mater.* **19**, 1918–1922 (2007).

10. P. S. Riseborough, J. M. Lawrence, Mixed valent metals. *Rep. Prog. Phys.* **79**, 084501 (2016).

11. K. Kuga, Y. Matsumoto, M. Okawa, S. Suzuki, T. Tomita, K. Sone, Y. Shimura, T. Sakakibara, D. Nishio-Hamane, Y. Karaki, Y. Takata, M. Matsunami, R. Eguchi, M. Taguchi, A. Chainani, S. Shin, K. Tamasaku, Y. Nishino, M. Yabashi, T. Ishikawa, S. Nakatsuji, Quantum valence criticality in a correlated metal. *Sci. Adv.* **4**, eaao3547 (2018).

12. L. Prochaska, X. Li, D. C. MacFarland, A. M. Andrews, M. Bonta, E. F. Bianco, S. Yazdi, W. Schrenk, H. Detz, A. Limbeck, Q. Si, E. Ringe, G. Strasser, J. Kono, S. Paschen, Singular charge fluctuations at a magnetic quantum critical point. *Science* **367**, 285–288 (2020).

13. A. Jayaraman, V. Narayanamurti, E. Bucher, R. G. Maines, Continuous and discontinuous semiconductor-metal transition in samarium monochalcogenides under pressure. *Phys. Rev. Lett.* **25**, 1430–1433 (1970).

14. I. Jarrige, H. Yamaoka, J. P. Rueff, J. F. Lin, M. Taguchi, N. Hiraoka, H. Ishii, K. D. Tsuei, K. Imura, T. Matsumura, A. Ochiai, H. S. Suzuki, A. Kotani, Unified understanding of the valence transition in the rare-earth monochalcogenides under pressure. *Phys. Rev. B* **87**, 115107 (2013).

15. Y.-F. Liao, B. Tegomo Chiogo, T. Clausse, T. Mazet, K.-D. Tsuei, D. Malterre, A. Chainani, Dual kondo effect charge ordering and zero thermal expansion in a correlated intermetallic. *Commun. Mater.* **3**, 23 (2022).

16. M. Ye, M. J. G. von Westarp, S.-M. Souliou, M. Peters, R. Möller, K. Kliemt, M. Merz, R. Heid, C. Krellner, M. Le Tacon, Strong electron-phonon coupling and enhanced phonon Grüneisen parameters in valence-fluctuating metal EuPd2Si2. *Phys. Rev. B* **107**, 195111 (2023).

17. S.-H. Jang, R. Sano, Y. Kato, Y. Motome, Antiferromagnetic Kitaev interaction in *f*-electron based honeycomb magnets. *Phys. Rev. B* **99**, 241106 (2019).

18. V. Chaturvedi, S. Ghosh, D. Gautreau, W. M. Postiglione, J. E. Dewey, P. Quarterman, P. P. Balakrishnan, B. J. Kirby, H. Zhou, H. Cheng, A. Huon, T. Charlton, M. R. Fitzsimmons, C. Korostynski, A. Jacobson, L. Figari, J. G. Barriocanal, T. Birol, K. A. Mkhoyan, C. Leighton, Room-temperature valence transition in a strain-tuned perovskite oxide. *Nat. Commun.* **13**, 7774 (2022).

19. A. Ramanathan, J. Kaplan, D.-C. Sergentu, J. A. Branson, M. Ozerov, A. I. Kolesnikov, S. G. Minasian, J. Autschbach, J. W. Freeland, Z. Jiang, M. Mourigal, H. S. La Pierre, Chemical design of electronic and magnetic energy scales of tetravalent praseodymium materials. *Nat. Commun.* **14**, 3134 (2023).

20. A. Ramanathan, E. D. Walter, M. Mourigal, H. S. La Pierre, Increased crystal field drives intermediate coupling and minimizes decoherence in tetravalent praseodymium qubits. *J. Am. Chem. Soc.* **145**, 17603–17612 (2023).

21. T. P. Gompa, A. Ramanathan, N. T. Rice, H. S. La Pierre, The chemical and physical properties of tetravalent lanthanides: Pr, Nd, Tb, and Dy. *Dalton Trans.* **49**, 15945–15987 (2020).

22. K. W. Brown, M. A. Plata, M. E. Raines, J. Y. Chan, Structural and Physical Properties of R2M3X5 Compounds, in *Handbook on the Physics and Chemistry of Rare Earth Elements*, J.-C. G. Bünzli, S. M. Kauzlarich, Eds. (Elsevier, 2023), vol. 64, chap. 330, pp. 1–92.

23. D. E. Bugaris, C. D. Malliakas, S. L. Bud'ko, N. P. Calta, D. Y. Chung, M. G. Kanatzidis, Flux crystal growth of the *RE*2Ru3Ge5 (RE = La, Ce, Nd, Gd, Tb) series and their magnetic and metamagnetic transitions. *lnorg. Chem.* **56**, 14584–14595 (2017).

24. L. G. Aksel'rud, Y. P. Yarmolyuk, E. I. Gladyshevskij, Kristallicheskaya structure soedineniya U2Co3Si5. *Kristallografiya* **22**, 861 (1977).

25. B. Chabot, E. Parthé, Dy2Co3Si5, Lu2Co3Si5, Y2Co3Si5 and Sc2Co3Si5 with a monoclinic Structural deformation variant of the orthorhombic U2Co3Si5 structure type. *J. Less-Common Met.* **106**, 53–59 (1985).

26. O. I. Bodak, B. Y. Kotur, V. I. Yarovets, E. I. Gladyshevskii, Kristallicheskaya struktura soedinenij Sc2Fe3Si5 i Dy2Fe3Si5. *Kristallografiya* **22**, 385–388 (1977).

27. D. E. Bugaris, C. D. Malliakas, F. Han, N. P. Calta, M. Sturza, M. J. Krogstad, R. Osborn, S. Rosenkranz, J. P. C. Ruff, G. Trimarchi, S. L. Bud'ko, M. Balasubramanian, D. Y. Chung, M. G. Kanatzidis, Charge density wave in the new polymorphs of RE2Ru3Ge5 (RE = Pr, Sm, Dy). *J. Am. Chem. Soc.* **139**, 4130–4143 (2017).

28. C. N. Kuo, C. J. Hsu, C. W. Tseng, W. T. Chen, S. Y. Lin, W. Z. Liu, Y. K. Kuo, C. S. Lue, Charge density wave like behavior with magnetic ordering in orthorhombic Sm2Ru3Ge5. *Phys. Rev. B* **101**, 155140 (2020).

29. R. Sokkalingam, G. Lingannan, M. Sundaramoorthy, C. S. Lue, C. N. Kuo, B. Joseph, S. Arumugam, Evidence of structural modulations induced by a charge density wave transition in orthorhombic Sm2Ru3Ge5. *Solid State Commun.* **372**, 115293 (2023).

30. Z. Li, X. Chen, X. Liu, Z. Yu, N. Su, Z. Liu, W. Xia, J. Jiao, C. Zhou, L. Zhang, Z. Dong, X. Wang, N. Yu, Z. Zou, J. Ma, J. Cheng, Z. Zhong, Y. Guo, Suppressed charge-density-wave, robust ferromagnetism and lifshitz transition in Sm2Ru3Ge5 crystal under high pressure. *J. Alloys Compd.* **937**, 168337 (2023).

31. Z. Hossain, H. Ohmoto, K. Umeo, F. Iga, T. Suzuki, T. Takabatake, N. Takamoto, K. Kindo, Antiferromagnetic kondo-lattice systems Ce2Rh3Ge5 and Ce2Ir3Ge5 with moderate heavy-fermion behavior. *Phys. Rev. B* **60**, 10383–10387 (1999).

32. S. Layek, V. K. Anand, Z. Hossain, Valence fluctuation in Ce2Co3Ge5 and crystal field effect in Pr2Co3Ge5. *J. Magn. Magn. Mater.* **321**, 3447–3452 (2009).

33. S. Ramakrishnan, A. Schönleber, T. Rekis, N. van Well, L. Noohinejad, S. van Smaalen, M. Tolkiehn, C. Paulmann, B. Bag, A. Thamizhavel, D. Pal, S. Ramakrishnan, Unusual charge density wave transition and absence of magnetic ordering in Er2Ir3Si5. *Phys. Rev. B* **101**, 060101 (2020).

34. S. Ramakrishnan, A. Schönleber, J.-K. Bao, T. Rekis, S. R. Kotla, A. M. Schaller, S. van Smaalen, L. Noohinejad, M. Tolkiehn, C. Paulmann, N. S. Sangeetha, D. Pal, A. Thamizhavel, S. Ramakrishnan, Modulated crystal structure of the atypical charge density wave state of single-crystal Lu2Ir3Si5. *Phys. Rev. B* **104**, 054116 (2021).

35. S. Ramakrishnan, J. Bao, C. Eisele, B. Patra, M. Nohara, B. Bag, L. Noohinejad, M. Tolkiehn, C. Paulmann, A. M. Schaller, T. Rekis, S. R. Kotla, A. Schönleber, A. Thamizhavel, B. Singh, S. Ramakrishnan, S. van Smaalen, Coupling between charge density wave ordering and magnetism in Ho2Ir3Si5. *Chem. Mater.*, **35**, 1980–1990 (2023).

36. T. M. Kyrk, J. P. Scheifers, K. Thanabalasingam, G. T. McCandless, D. P. Young, J. Y. Chan, It runs in the BaAl4 family: relating the structure and properties of middle child

Ln2Co3Ge5 (Ln = Pr, Nd, and Sm) to its siblings LnCo2Ge2 and LnCoGe3. *lnorg. Chem.* **60**, 15343–15350 (2021).

37. T. M. Kyrk, J. Galeano-Cabral, E. R. Kennedy, K. Wei, G. T. McCandless, M. C. Scott, R. E. Baumbach, J. Y. Chan, Anisotropic magnetic and transport properties of orthorhombic *o*-Pr2Co3Ge5. *J. Phys. Mater.* **5**, 044007 (2022).

38. A. Gulec, D. Phelan, C. Leighton, R. F. Klie, Simultaneous first-order valence and oxygen vacancy order/disorder transitions in (Pr0.85Y0.15)0.7Ca0.3CoO3−δ via analytical transmission electron microscopy. *ACS Nano* **10**, 938–947 (2016).

39. P. Weidner, K. Keulerz, R. Löhe, B. Roden, J. Röhler, B. Wittershagen, D. Wohlleben, High temperature susceptibility, valence and volume anomaly of some Ce-compounds. *J. Magn. Magn. Mater.* **47–48**, 75–78 (1985).

40. R. M. White, P. Fulde, Excitonic mass enhancement in praseodymium. *Phys. Rev. Lett.* **47**, 1540–1542 (1981).

41. V. K. Anand, Z. Hossain, C. Geibel, Magnetic order in Pr2Pd3Ge5 and possible heavy-fermion behavior in Pr2Rh3Ge5. *Phys. Rev. B* **77**, 184407 (2008).

42. T. A. Sayles, R. E. Baumbach, W. M. Yuhasz, M. B. Maple, Ł. Bochenek, R. Wawryk, T. Cichorek, A. Pietraszko, Z. Henkie, P.-C. Ho, Superconductivity and crystalline electric field effects in the filled skutterudite PrRu4As12. *Phys. Rev. B* **82**, 104513 (2010).

43. A. Sakai, S. Nakatsuji, Kondo effects and multipolar order in the cubic PrTr2Al20 (Tr=Ti, V). *J. Phys. Soc. Jpn.* **80**, 063701 (2011).

44. J. Otsuki, H. Kusunose, Y. Kuramoto, Theory of crystalline electric field and Kondo effect in Pr skutterudites. *J. Physical Soc. Jpn.* **74**, 200–208 (2005).

45. V. J. Yannello, D. C. Fredrickson, Generality of the 18-n rule: Intermetallic structural chemistry explained through isolobal analogies to transition metal complexes. *Inorg. Chem.* **54**, 11385–11398 (2015).

46. V. Svitlyk, W. Hermes, B. Chevalier, S. F. Matar, E. Gaudin, D. Voßwinkel, D. Chernyshov, R.-D. Hoffmann, R. Pöttgen, Change of the cerium valence with temperature – Structure and chemical bonding of HT-CeRhGe. *Solid State Sci.* **21**, 6–10 (2013).

47. D. Zhang, A. O. Oliynyk, A. Mar, Three Rh-rich ternary germanides in the Ce–Rh−Ge system. *J. Solid State Chem.* **304**, 122585 (2021).

48. R. Freccero, P. Solokha, S. De Negri, A. Saccone, Y. Grin, F. R. Wagner, Polar-covalent bonding beyond the zintl picture in intermetallic rare-earth germanides. *Chemistry* **25**, 6600–6612 (2019).

49. R. Freccero, S. De Negri, G. Rogl, G. Binder, H. Michor, P. F. Rogl, A. Saccone, P. Solokha, La2Pd3Ge5 and Nd2Pd3Ge5 compounds: Chemical bonding and physical properties. *Inorg. Chem.* **60**, 3345–3354 (2021).

50. R. Freccero, L. C. J. Pereira, P. Solokha, S. De Negri, Flux growth, crystal structure, and chemical bonding of Yb2PdGe3, an AlB2 superstructure within the rare-earth series. *lnorg. Chem.* **62**, 1988–1999 (2023).

51. Y. Lai, K. Wei, G. Chappell, J. Diaz, T. Siegrist, P. J. W. Moll, D. Graf, R. E. Baumbach, Tuning the structural and antiferromagnetic phase transitions in UCr2Si2: Hydrostatic pressure and chemical substitution. *Phys. Rev. Mater.* **4**, 075003 (2020).

52. U. Subbarao, S. C. Peter, Crystal growth and properties of YbCuGa3: First monoclinic system in the RETX3 family. *Cryst. Growth Des.* **13**, 953–959 (2013).

53. A. Imre, A. Hellmann, A. Mewis, LaPt2Ge2 und EuPt2Ge2 –Neubestimmung der Kristallstrukturen. *Z. Anorg. Allg. Chem.* **632**, 2217–2221 (2006).

54. A. Lim, D. C. Fredrickson, Entropic control of bonding, guided by chemical pressure: Phase transitions and 18-*n*+*m* isomerism of IrIn3. *Inorg. Chem.* **62**, 10833–10846 (2023).

55. P. Canfield, T. Kong, U. Kaluarachchi, N. H. Jo, Use of Frit-disc crucibles for routine and exploratory solution growth of single crystalline samples. *Philos. Mag.* **96**, 84–92 (2016).

56. T. M. Kyrk, M. Bravo, G. T. McCandless, S. H. Lapidus, J. Y. Chan, Investigating the An+1BnX3n+1 homologous series: A new platform for studying magnetic praseodymium based intermetallics. *ACS Omega* **7**, 19048–19057 (2022).

57. J. Herrero-Martín, J. L. García-Muñoz, S. Valencia, C. Frontera, J. Blasco, A. J. Barón-González, G. Subías, R. Abrudan, F. Radu, E. Dudzik, R. Feyerherm, Valence change of praseodymium in Pr0.5Ca0.5CoO3 investigated by X-ray absorption spectroscopy. *Phys. Rev. B* **84**, 115131 (2011).

58. Q. Lu, G. Vardar, M. Jansen, S. R. Bishop, I. Waluyo, H. L. Tuller, B. Yildiz, Surface defect chemistry and electronic structure of Pr0.1Ce0.9O2−δ revealed in operando. *Chem. Mater.* **30**, 2600–2606 (2018).

59. P. Solokha, R. Freccero, S. De Negri, D. M. Proserpio, A. Saccone, The R2Pd3Ge5 (R = La–Nd, Sm) Germanides: Synthesis, crystal structure and symmetry reduction. *Struct. Chem.* **27**, 1693–1701 (2016).

60. B. Chabot, E. Parthé, Ce2Co3Si5 and R2Ni3Si5 (R = Ce, Dy, Y) with the orthorhombic U2Co3Si5-type structure and the structural relationship with the tetragonal Sc2Fe3Si5-type structure. *J. Less-Common Met.* **97**, 285–290 (1984).

61. B. Chevalier, T. Roisnel, J. Etourneau, Magnetic structure of U2(Ru0.65Rh0.35)3Si5 silicide. *J. Magn. Magn. Mater.* **134**, 88–94 (1994).

62. T. Kawai, H. Muranaka, T. Endo, N. Duc Dung, Y. Doi, S. Ikeda, T. D. Matsuda, Y. Haga, H. Harima, R. Settai, Y. Ōnuki, Split fermi surface properties of LaTGe3 (T: Transition Metal) and PrCoGe3 with the non-centrosymmetric crystal structure. *J. Phys. Soc. Jpn.* **77**, 064717 (2008).

63. A. Szytula, J. Leciejewicz, H. Bińczycka, Crystal and magnetic structures of PrCo2Ge2 and HoCo2Ge2. *Phys. Stat. Sol. A* **58**, 67–70 (1980).

64. M. Rahm, R. Hoffmann, N. W. Ashcroft, Atomic and ionic radii of elements 1–96. *Chem. A Eur. J.* **22**, 14625–14632 (2016).

65. H. Fukuoka, K. Baba, M. Yoshikawa, F. Ohtsu, S. Yamanaka, High-pressure synthesis and structures of lanthanide germanides of LnGe5 (Ln=Ce, Pr, Nd, and Sm) isotypic with LaGe5. *J. Solid State Chem.* **182**, 2024–2029 (2009).

66. H. Fukuoka, M. Yoshikawa, K. Baba, S. Yamanaka, Preparation and structures of lanthanoid germanides, PrGe3.36, NdGe3.25, and TmGe3 with double square Ge-Mesh structures. *Bull. Chem. Soc. Jpn.* **83**, 323–327 (2010).

67. J. Liu, V. Smetana, K. A. G. Jr., G. J. Miller, V. K. Pecharsky, The crystal structure and magnetic properties of Pr117Co56.7Ge112. *J. Appl. Phys.* **113**, 17E120 (2013).

68. S. Skanthakumar, J. W. Lynn, C. Mazumdar, R. Nagarajan, L. C. Gupta, Magnetic phase transitions in R2Ni3Si5. *Physica B* **241–243**, 693–695 (1997).

69. A. Gil, M. Kolenda, S. Baran, B. Penc, M. Hofmann, A. Szytuła, Neutron diffraction studies of R2Co3Si5 (R = Tb,Dy) and Tb2Ir3Si5 compounds. *Physica B Condens. Matter* **276-278**, 742–743 (2000).

70. L. Durivault, F. Bourée, B. Chevalier, G. André, J. Etourneau, Magnetic ordering in the ternary germanide Ce2Ni3Ge5 as studied by neutron powder diffraction. *J. Magn. Magn. Mater.* **246**, 366–374 (2002).

71. V. K. Anand, D. T. Adroja, C. Ritter, D. Das, H. S. Nair, A. Bhattacharyya, L. Liborio, S. Sturniolo, F. L. Pratt, D. Le, G. Andre, H. Luetkens, A. D. Hillier, Z. Hossain, Magnetic structure and crystal field states of Pr2Pd3Ge5: μSR and neutron scattering investigations. *Phys. Rev. B* **107**, 104412 (2023).

72. N. N. Efremova, Praseodymium valence state in PrFe10Mo2, PrNi5, and PrNi4*M* intermetallic compounds (*M* = Cu, Al, Ga). *Phys. Solid State* **47**, 424–428 (2005).